Optical diagnostics for a ring resonator free-electron laser

Mary L. Laucks, MEMBER SPIE
David H. Dowell
Andrew R. Lowrey
Boeing Defense and Space Group
Mail Stop 2T-50
P.O. Box 3999
Seattle, WA 98124

Steven C. Bender
Alex H. Lumpkin,* MEMBER SPIE
Los Alamos National Laboratory
P.O. Box 1663
Los Alamos, New Mexico 87545

Melvin P. Bentz
Rocketdyne Division of Rockwell International
6633 Canoga Avenue
Canoga Park, California 91303

Abstract. The optical cavity of the Boeing free-electron laser (FEL) was reconfigured as a semiconfocal ring resonator with two glancing incidence hyperboloid–paraboloid telescopes. The challenge for this experiment was the complexity of the ring resonator compared to the simplicity of a concentric cavity. The ring resonator's nonspherical mirror surfaces, its multiple elements, and the size of the components contributed to the problems of keeping the optical mode of the resonator matched to the electron beam in the wiggler. Several new optical diagnostics were developed to determine when the optical mode in the FEL was spatially and temporally matched to the electron beam through the wiggler. These included measurements of the focus position and Rayleigh range of the ring resonator optics to determine the spatial match of the optical mode through the wiggler, and a measurement of the position of the optical axis for multiple passes around the ring resonator to determine the stability of the resonator alignment. This paper also describes the optical measurements that were necessary to achieve reliable lasing. The techniques for measuring ring resonator Rayleigh range and focus position, multiple pass alignment, cavity length, optical energy per micropulse, peak power, optical extraction, small signal gain, ringdown loss, lasing wavelength, electron bunch pulse width, and energy slew are discussed.

Subject terms: optical diagnostics; ring resonators; free-electron lasers.

Optical Engineering 32(2), 384–394 (February 1993).

1 Overview of Experiment

Boeing's visible free-electron laser (FEL) program was proposed as a three-step process to demonstrate the feasibility of high average power FELs. In the first step a visible, concentric cavity, FEL oscillator was built and tested. It was a high peak power, but low average power device. In 1987 this experiment achieved the shortest wavelength radiation (0.50 μm) from any rf accelerator-driven oscillator.[1] Sideband generation was demonstrated both in the 4% tapered wiggler and in the untapered wiggler. Measurements with the untapered wiggler indicated extraction efficiencies up to 0.25%, whereas extraction efficiencies of up to 0.75% were seen in the 4% tapered wiggler.[2,3]

In the next phase, begun in mid 1989, the optical cavity was reconfigured to test the design of a glancing incidence ring resonator. The mirrors in the optical cavity were placed at glancing incidence to be able to operate under high average power optical beams.[4,5] First lasing with a ring resonator FEL occurred at 630 nm in March 1990.[6,7] The ring resonator diagnostics were improved to include the ability to measure the focus position, Rayleigh range, and walking modes of the resonator and the quality of lasing much improved.

The third experiment was to have been the construction and testing of a high average power master oscillator power amplifier (HAP MOPA) FEL. Instead, at this time, design of a 10-μm, 100-kW average power laser experiment (APLE) and experimental work on the injector for APLE continue.[8,9]

The crucial requirement for lasing to occur in an FEL is that the electron beam and the optical mode supported in the ring resonator overlap spatially and in time. The electron accelerator must produce a beam that is the right size and brightness and is matched into the wiggler. The resonator, in turn, must provide an optical mode with the correct size at the center of the wiggler and the appropriate Rayleigh range to maintain overlap. Once the optical mode was cor-

*Present affiliation: Argonne National Laboratory, 9700 South Cass Avenue, Argonne, Illinois 60439-4814.

Paper 14121 received Dec. 12, 1991; revised manuscript received June 11, 1992; accepted for publication June 12, 1992. This paper is a revision of a paper presented at the SPIE conference on Design, Modeling, and Control of Laser Beam Optics, January 1992, Los Angeles, Calif. The paper presented there appears (unrefereed) in SPIE Proceedings Vol. 1625.

rect, the optical axis of the resonator could be aligned to the wiggler axis with the help of apertures on either side of the wiggler that defined the overall reference line for the FEL. Temporal overlap was achieved by tuning the cavity length of the resonator to match the separation in time of the electron beam micropulses. The requirements for overlap were derived from FEL interaction simulations and were taken to be less than 100 μm for decentering of the electron bunch and optical pulse axes, less than 6 μm for desynchronism, and less than 20 μrad of tilt between the two axes.

The layout of the ring resonator oscillator experiment is shown in Fig. 1 and a summary of its design parameters is shown in Table 1.[5,6]

Accelerator. The FEL oscillator was driven by an L-band rf traveling-wave linear accelerator. Electrons were bunched by two standing-wave cavity prebunchers (at 108 and 433 MHz) and a tapered phase velocity cavity (at 1300 MHz),[10] accelerated to 110 MeV and then transported to the 5-m adjustable-taper wiggler through a 180-deg achromatic, nonisochronous bend. Electrons were ejected by a thermionic gun in a "burst" format. The macropulses were 150 to 200 μs long and occurred at a 2-Hz rate. At the entry to the accelerator the micropulses contained 5 nC of charge in 10 to 15-ps bunch and were separated by 433 ns. After being transported to the wiggler the micropulse charge had dropped to about 3 nC, making available up to 300 A of peak current in the wiggler.

Wiggler. Spectra Technology Incorporated (STI) designed and built the wiggler for the FEL oscillator experiment.[11] The 5-m taperable hybrid undulator (THUNDER) was linearly polarized in the horizontal plane. It was constructed in ten 50-cm-long segments of samarium-cobalt magnets interleaved with vanadium Permendur on trays above and below a 4.76-mm-bore vacuum beam pipe. Between each subsection of the wiggler were diagnostics stations with a retractable optical transition radiation (OTR) screen and a viewing port, a beam position monitor, and a steering coil. The wiggler could be adjusted to give up to a 12% taper in axial magnetic field strength. However, for the experiment described, the wiggler was uniform.

Ring resonator (Fig. 2). The ring resonator was designed and built by the Rocketdyne Division of Rockwell International and contained two grazing incidence reflective telescopes (7× magnification), each formed by a grazing incidence hyperboloid mirror ($f = -105$ cm) and its companion off-axis paraboloid mirror ($f = 698$ cm).[4] The resonator was closed by two flats: one used for dynamic jitter correction and the other used to outcouple some of the circulating beam. The downstream telescope collimated and expanded the spontaneous light to a 10-cm-diameter beam and sent it upstream to an identical telescope, which then focused it at the midpoint of the wiggler. The waist size of the beam at the midpoint of the wiggler was 0.7 mm and the Rayleigh range of the ring resonator was 240 cm. The outcoupler's transmission was a steeply increasing function of wavelength above 635 nm and so the outcoupler acted as an edge filter for wavelengths above 635 nm and acted to suppress FEL sidebands. The combined losses of the other optical elements was about 25%, and the loss of the outcoupler at 635 nm due to transmission was about 5%, so the wavelength of FEL radiation had to be below 635 nm to keep the total resonator losses below 30%.

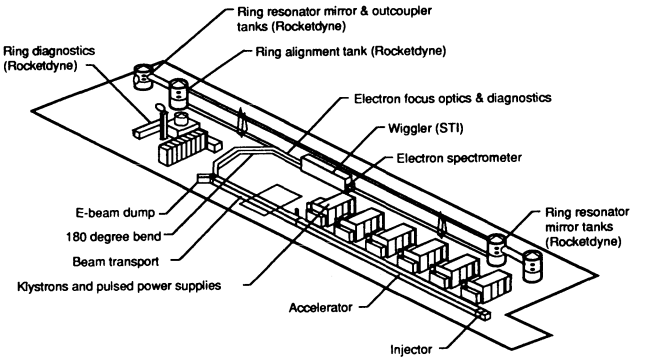

Fig. 1 Layout of Boeing's FEL oscillator experiment.

Table 1 Design parameters of the ring resonator.

Electron Beam	
Electron Beam Energy	110 MeV
Repetition Rate	2 Hertz
Macropulse Length	110 microseconds
Micropulse Spacing	443 nanoseconds
Emittance ($4\varepsilon_{rms}$)	100-120 π mm mrad
Macropulse Energy Jitter	0.5% - 0.75% FWHM
Micropulse Energy Spread	0.5% FWHM
Micropulse Width	12 picoseconds FWHM
Micropulse Charge	3 nanocoulombs
Wiggler	
Length	5 m in 10, 50 cm sections
Wiggler Period	2.18 cm
Number of Periods	220
Peak Magnetic Field	10.2 KGauss
Wiggler parameter	1.8 (peak)
	1.31 (rms)
Betratron Period	5.6 m
Ring Resonator	
Rayleigh Range	240 cm
Hyperboloid Focal Length	-105 cm
Paraboloid Focal Length	698 cm
Telescope Magnification	7x
Hyperboloid-Paraboloid Spacing	600 cm
Roundtrip Path Length	133 m , 443 ns

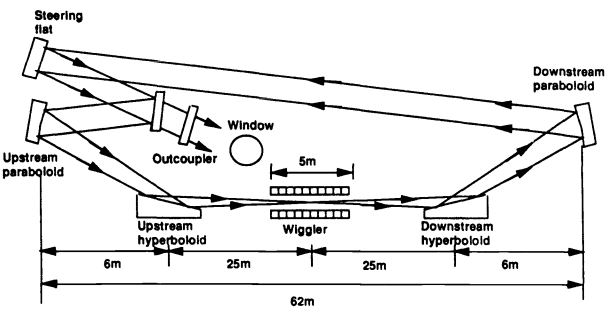

Fig. 2 Grazing incidence ring resonator.

Optical cavity stabilization. Dynamic control of the resonator alignment and cavity length was accomplished by an electro-optical servo system. A HeNe laser was injected near the center of the wiggler and traveled counterclockwise off-axis around the resonator, ending on a quadrant detector on the opposite side of the wiggler. The signal from the quadrant detector acted as the feedback control for the fast steering mirror shown in Fig. 2. STI designed and built the

Table 2 Summary of FEL optical measurements.

MEASUREMENT	PURPOSE	DETECTOR	ERROR	SOURCE
Focus position	Focus position of optical mode supported in the ring	Digitizing camera	+/- 0.5m	FWHM calculation, astigmatism in beam, positioning of camera
Multi-pass Alignment	Successive passes around ring are made colinear	Digitizing camera	350 microns	Stabilization system
Energy per Micropulse	Extracted optical power, peak power, average power	Vacuum Photodiode	22%	Detector response, cable response, optical path
Small signal gain	FEL gain before saturation	Photomultiplier tube	variable	Scope triggering
Ringdown loss	Ring losses for optical extraction	Vacuum photodoide, Silicon photodoide	< 5%	Reading errors
Wavelength	Extracted optical power, electron energy	Optical multichannel analyzer, streak monochromator	< 1%	Calibration, resolution of monochromator
Pulse width	Wiggler current, prebuncher tuning	Streak camera	10%	Statistical, systematic in electron beam
Cavity length search	Synchronism of light and electron bunchers	Streak camera	200 microns	Streak camera, electron beam variations

quadrant cell and the transport optics; the servo system was designed and built by Rocketdyne. The response function of the servo system showed that it suppressed noise to 30 Hz only. The remaining jitter at the center of the wiggler was 350 to 500 μm, peak-to-peak, which came from frequency components at 50 and 100 Hz.

Diagnostics. The diagnostics used during the experiment are summarized in Table 2, which includes an estimate of the measurement errors.

2 Resonator Alignment

The resonator optics were initially aligned by two beams from a HeNe laser and a self-referencing interferometer system. Figure 3(b) is a diagram of the injection optics for the two alignment beams.[5] A 30-mW HeNe laser polarized in the horizontal plane was spatially filtered by an elliptical pinhole (so as to be round at the hologram) before it was injected into the alignment tank where a hologram split the beam into a forward and reverse beam propagating around the ring resonator. The two alignment beams were mode-matched to the resonator by the hologram. A second hologram picked off a piece of the forward propagating beam and transported it back to a self-referencing interferometer. The interferometer system allowed wavefront aberrations to be analyzed,[12] but was insensitive to the resonator's focus position and Rayleigh range.

To assure that the optical mode in the resonator was correct, the focus position and Rayleigh range of the resonator were determined. However, because the injection optics for the alignment beam added aberrations that were not present in the resonator, the only measurable quantities were the focus position and Rayleigh range of the forward and reverse propagating alignment beams. The focus position and Rayleigh range of the ring resonator could be derived in the way described below in Sec. 2.1. The measurement of pass-to-pass alignment of the resonator assured that the ring resonator was stable pass to pass, as described in Sec. 2.2.

2.1 *Focus Position and Rayleigh Range*

Figure 3(a) illustrates the focus position measurement of the forward (source) and reverse (image) alignment beams. The forward propagating beam was turned out of the resonator pipe by a retractable mirror in front of the wiggler. The beam then traveled outside the resonator a distance equal to the distance it would have traveled through the wiggler. A digitizing camera was moved on a tripod along this virtual wiggler in half-meter increments and recorded the full width half-maximum (FWHM) of the beam spot at each position. The reverse propagating beam was measured in a similar way. In this case, the beam propagated around the resonator and was turned out by a retractable mirror just downstream of the wiggler. An example of the data from these measurements is shown in Fig. 4. The FWHM spot sizes were fit with a least-squares routine to give the focus position, waist size, and Rayleigh ranges of the two alignment beams. With this information graphs like the one in Fig. 5 were generated. To determine the Rayleigh range (z_R) of the ring resonator from this graph, a horizontal line is drawn from the right axis at the value of the image's (i.e., the reverse hologram beam's) Rayleigh range. Where this line intersects each z_R curve, a perpendicular line is dropped from the intersection point to the corresponding focus position curve. A line drawn through all these points on the focus position curves defines the solution curve. The point where this curve intersects the appropriate horizontal line drawn from the left axis will fall on a unique ring resonator Rayleigh range curve. This curve is the Rayleigh range of the resonator as determined from the two alignment beams. If the intersection point falls on a curve below the curve representing $z_R = 0.0$, the resonator will be unstable.

The focus position of the ring resonator was inferred from the horizontal axis of the graph. The horizontal axis represents the distance from the resonator waist to the source focus position. Downstream is positive on this axis. The source focus position as determined from the solution curve is the position of the source focus relative to the waist position of the resonator. If the location of the source focus

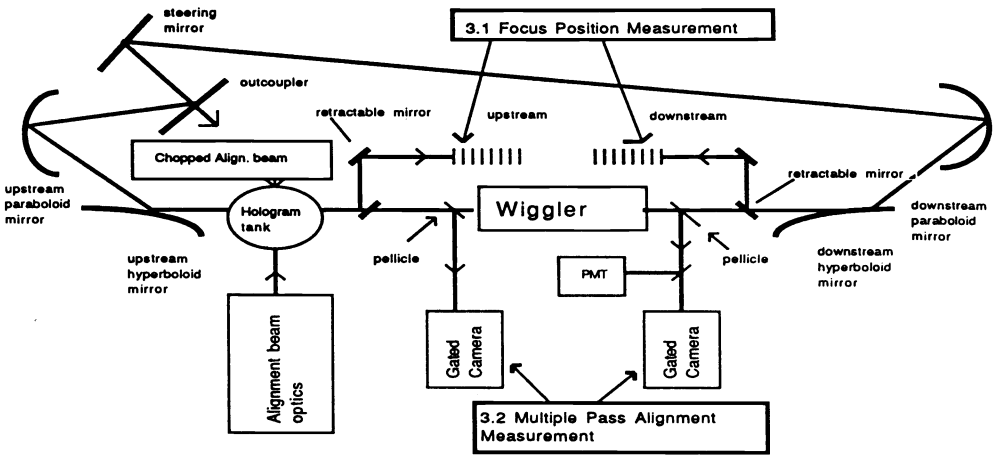

(a)

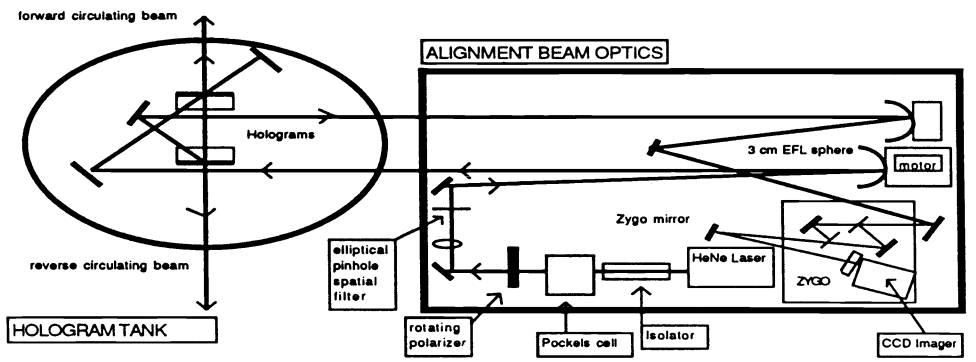

(b)

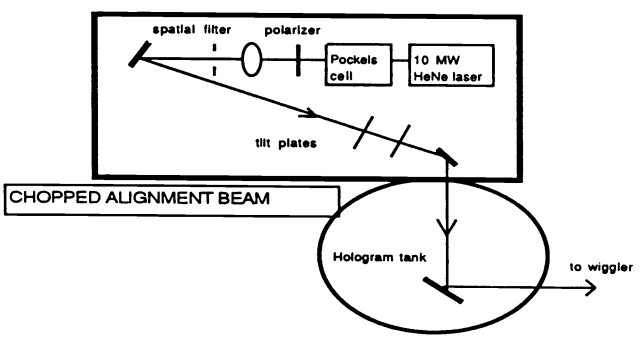

(c)

Fig. 3 Alignment diagnostics for the ring resonator.

relative to the physical midpoint of the wiggler is known, the waist position of the resonator relative to the physical midpoint of the wiggler can be determined.

The standard deviation of the spot size measurements at each camera position was about 4%. However, several systematic errors were involved in this measurement. Astigmatism in the input optics of the alignment beam caused the focus position to be different in the horizontal and vertical planes. Another systematic error occurred in the way that the video analysis program calculated the FWHM of the beam spots. If there were other aberrations in the spot so that the intensity distribution of the beam spot was not regular, errors in the calculation of the FWHM resulted. Also, the fitting routine assumed that the functional relationship between spot size and position was Gaussian, but in reality many of the curves required an additional parameter because of the asymmetry of the curves. Since the reduced χ^2 for the fits was about 25, an estimate of the error in this measurement was obtained by multiplying 4% by the square root of 25 (since chi squared is proportional to sigma squared). Therefore, the focus position uncertainty was 20%, or a meter in a 5-m wiggler.

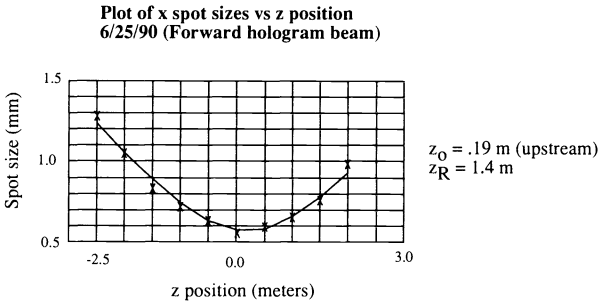

Fig. 4 Focus position data.

2.2 *Multiple-Pass Alignment*

Simulations of multiple passes of the propagating optical mode in the ring resonator indicated that the optical mode would oscillate from side to side of the resonator axis if it had been injected into the resonator with an initial offset or at an angle. A characteristic of these oscillations was that successive passes would be on opposite sides of the resonator axis, unlike in the behavior in the concentric cavity where successive passes would merely drift toward one side and back over many passes. This behavior in the ring resonator made the startup of lasing difficult if there was sufficient misalignment. The multiple-pass alignment diagnostic was meant to detect the offsets of successive passes from the resonator axis so that the alignment of the resonator optics could be corrected.

A diagram of the multipass alignment measurement is shown in Fig. 3(a). The alignment laser was chopped by the Pockels cell shown on the alignment table in Fig. 3(c). The chopped alignment beam was turned out of the beamline by two pellicles in front of and at the exit of the wiggler (Fig. 3(a)). Two gated cameras were timed to detect successive passes. About 8 passes could be detected by the gated cameras. Two cameras gave the measurement added sensitivity. The gated camera's output was digitized so that the FWHM of the chopped beam and its displacement from the wiggler axis could be recorded. The standard deviations of the offset and FWHM data were between 1 and 5% for the first pass, and up to 50% for the last pass seen by the camera, because of low light levels and the associated digitizing problems. Jitter in the stabilization system that maintained the position of the resonator optics and the alignment beam was about 300 μm. However, by averaging the centroid values of the multiple passes, the centroid position of the beam could be determined to better than 30 μm. To correct for large excursions from the wiggler axis, the outcoupler, downstream paraboloid mirror, or fast steering mirror was tipped or tilted.

3 Cavity Length Search

The electron beam bunches were spaced 443 ns apart and so the time of flight of the optical pulses around the ring resonator had to be exactly equal to 443 ns for lasing to occur. If the optical cavity length of the resonator was not set correctly, optical bunches from separate passes around the ring would not coincide. The cavity length was usually fine-tuned by moving the outcoupler flat along the optical axis of the resonator.

The length of the ring resonator was set to within a few millimeters when the resonator hardware was initially installed. To set the length to micrometers, a streak camera was used to detect the spacing between multiple passes around the resonator of the outcoupled spontaneous emission. Because the pulse width of the spontaneous emission was about 15 ps, it was not possible to resolve pulse spacings smaller than this number. This meant that the uncertainty for one measurement was nearly 3 mm. However, if the pulse separation was measured for various outcoupler positions along the resonator axis and a linear fit was made to the data, it was possible to predict the correct position of the outcoupler to within 200 μm. A fine search (in 10-μm steps) was then made on either side of the predicted position. A scan that was made before the first lasing occurred in March 1990 is shown in Fig. 6. The top box in the figure shows a typical streak camera measurement of desynchronism.

4 Energy per Micropulse

If the energy per micropulse, pulse width, and wavelength of the optical pulse from the FEL are known, then peak power and optical extraction can be calculated. The outcoupled energy per micropulse measurement was made with a biplanar vacuum photodiode (VPD) (Hamamatsu R1193U), which was located in the chamber near the outcoupler window (see Fig. 13). The detector response was linear over several orders of magnitude and was fast enough to separate individual micropulses. An example of the data is shown in Fig. 7. The peak voltage of the detector was measured with an oscilloscope and was used to determine the energy per micropulse given by

$$E_{\text{per micropulse}} = (V_{\text{peak}} \cdot 10^{\text{ND}})/(R_\lambda R_{V/Q} \text{OP}) \ , \qquad (1)$$

where V_{peak} is the peak voltage of vacuum photodiode in control room, ND is the optical density of neutral density filter, OP is the optical path loss, R_λ is the responsivity of vacuum photodiode at 630 nm, nC/nJ; and $R_{V/Q}$ is the instrumentation calibration. Measured values of energy per micropulse ranged from 300 nJ on 23 March 1990 to 30 μJ on 12 October 1990.

R_λ, OP, and $R_{V/Q}$ were determined by calibrating the detector, optical path, and instrumentation independently. The detector had both a dc and an impulse response. EG&G at Los Alamos calibrated the dc spectral response for the Hamamatsu vacuum photodiode with a spectral radiometer system. A known quantity of monochromatic light illuminated the photocathode and the current was measured with a computer-controlled electrometer. The responses for 630 and 620 nm differ by only 9%, so the value for 630 nm (0.0312 nC/nJ) was used for all wavelengths between 625 and 635 nm.

The impulse response of the detector is the charge-to-voltage ratio of the signal pulse of the detector. This ratio is highly dependent on the instrumentation used. EG&G provided an estimate of the saturation level of the VPD, defined as the highest level that the addition of a ND filter of 0.3 will reduce the output by 50%. Indirectly this was also a check that there are no pulse effects (e.g., space charge) that would affect the dc spectral responsivity. The results of these measurements indicated that the photodiode

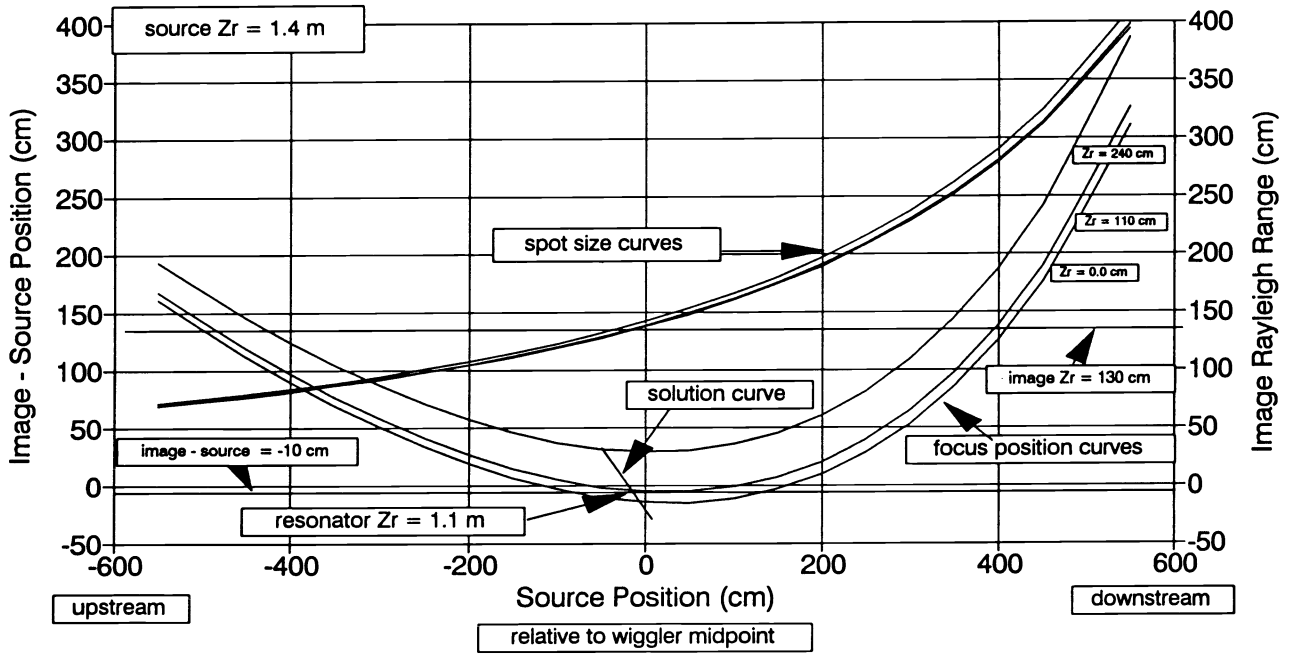

Fig. 5 Resonator Rayleigh range.

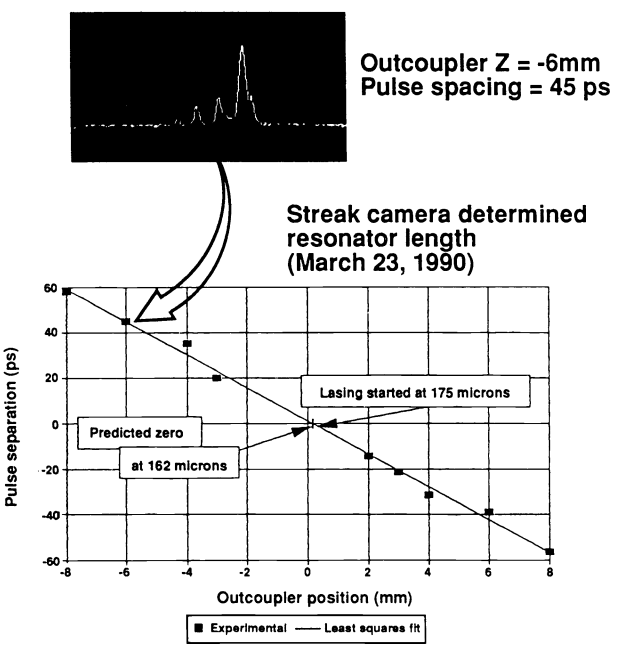

Fig. 6 Cavity length search.

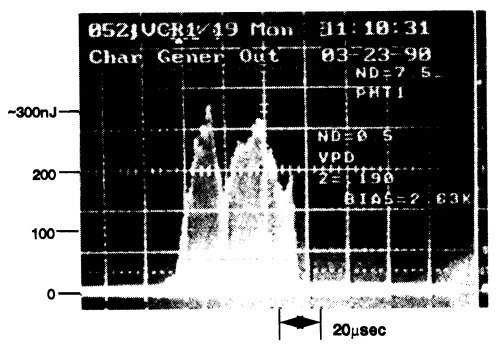

Fig. 7 Energy per micropulse.

saturated at about 8 nJ when operated at a bias voltage of 2.5 kV at 632 nm.

The applied bias voltage had an effect on the impulse response of the VPD but not on the dc spectral response. The recommended operating bias was about 2.5 kV. Variations of the bias between 2.0 and 2.5 kV had only a 7% effect on the signal voltage. The calibration of the optical path between the outcoupler window and the VPD was complicated by the fact that the outcoupled beam had a large diameter. The path was calibrated in two stages. The first flat and the beamsplitter were calibrated separately from the rest of the optical path using a HeNe laser polarized in the x plane to simulate the FEL light. To simulate the larger beam the measurement was repeated at different positions on the optics. The rest of the path was calibrated using the actual ring alignment laser. All calibrations were done with an optical power meter (Newport model 835).

The instrumentation calibration consisted of four parts: the dc loss of the signal cable, the dc loss of the bias cable, the pulsed response of the cable, and the response of the oscilloscope used to measure the signal. The signal cable from the chamber was RG-213 and the bias cable was RG-59. The power supply for the bias was in the control room and the signal was measured on an oscilloscope (7104 Tektronix). The dc loss of both the signal and bias cables was determined to be negligible. The VPD had a 50-Ω resistor

across the output and so the total effective resistance that the signal saw when put into a 50-Ω oscilloscope was 25-Ω. The pulsed cable response was checked with a fast pulser (1 ns) and found to give $Q_{in}/Q_{out} = 1.0$ to within 10%. The oscilloscope response was determined by calculating the peak-to-area ratio of the VPD signal. The combined errors in the overall calibration of the energy per micropulse detector were 22%.

Once the energy per micropulse of the FEL light was known, several important laser parameters could be derived. Outcoupled peak power was obtained by dividing the energy per micropulse by the pulse width of the micropulse, usually 9 ps. Using the numbers for energy per micropulse above, outcoupled peak power ranged from 33 kW to 3 MW.

Optical extraction, η, a measure of how efficient the conversion of electron energy to optical energy was in the FEL interaction, was given by

$$\eta = (E_\lambda L_{RD})/(E_e T_{oc}) \ , \tag{2}$$

where E_λ is the outcoupled optical energy in one micropulse, L_{RD} is the micropulse ring loss, E_e is the electron beam energy in one micropulse, and T_{oc} is the transmission of the outcoupler at λ. The best value of extraction efficiency achieved was 0.028% on 11 October 1990. This should be compared to the value of 0.2% achieved on 21 February 1989 with the untapered wiggler and concentric cavity resonator.[2,3]

5 Small Signal Gain

The gain of an FEL in the small signal regime is an asymmetric function of the electron energy and was first measured by Madey and coworkers in 1977.[13] The small signal gain (SSG) of an FEL determines whether lasing can occur. If the small signal gain is larger than the combined losses in the ring resonator, lasing can occur.

Net SSG (SSG − resonator losses) was measured by a photomultiplier tube (Hamamatsu R955) near the outcoupler window on the chamber diagnostics table (see Fig. 13). The photomultiplier had sufficient sensitivity to allow the detection of spontaneous emission. SSG was measured at the beginning of the micropulse where the first enhanced micropulses could be seen. The laser signal was not attenuated in order to make sure the gain was measured in the small signal region, at least a factor of 10,000 below laser saturation.

This measurement had several difficulties that led to large and variable experimental errors. One was that if lasing occurred near the beginning of the macropulse, much of the variation in gain was due not to the lasing interaction but to instabilities in the accelerator rf over the first 5 to 10 μs of the macropulse. A further difficulty was how to trigger the measurement oscilloscope. Because the position in the macropulse where lasing occurred varied, a fixed window delay could not be established that would work for every macropulse. When lasing was erratic it was difficult to capture SSG data. An example of SSG data is shown in Fig. 8. From the data, net small signal gain per pass, SSG_{net}, can be calculated by

$$SSG_{net} = (1/N)\ln(A/A_0) \ , \tag{3}$$

where N is the number of passes, A is the amplitude of the N'th pass, and A_0 is the amplitude of the initial pass.

Fig. 8 Small signal gain.

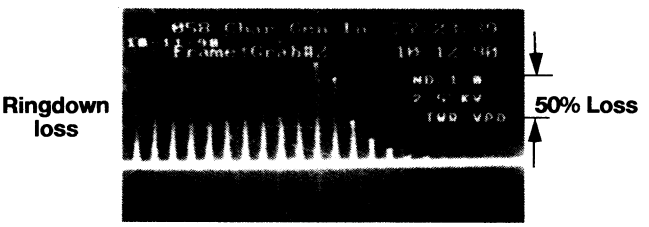

Fig. 9 Ringdown loss.

6 Ringdown Loss

Both optical cavity losses and losses due to e-beam variations and misalignments suppressed FEL gain. Optical cavity losses were made up of the combined diffractive and absorptive losses from optical surfaces, misalignments, jitter, aperturing through the wiggler of the optical mode, and mode mismatches. Optical cavity losses were measured with the chopped alignment beam and a photomultiplier tube (Hamamatsu R955) in the same location where the cameras for multipass alignment are positioned (see Fig. 3(a)).

The loss measured between the pulses present in the ring resonator after the last electron beam micropulse (the ringdown pulses) was a good indication of the combined resonator and electron beam losses in the FEL interaction. These pulses were measured with the vacuum photodiode described above for the energy per micropulse measurement. It was important that the diode be checked for saturation before the ringdown measurement was made. A 0.3 ND filter was inserted in front of the detector to check that the amplitude of the signal fell by half. In Fig. 9, ringdown data are pictured. Ringdown loss is calculated by the same formula as SSG_{net} except with a minus sign to account for the fact that A_0 is greater than A. Because this was a relative measurement, the errors were relatively small (less than 5% if the detector was not in saturation) and came from reading errors on the oscilloscope.

7 Wavelength

An optical multichannel analyzer (OMA) (EG&G Princeton Applied Research Model 1460) was used in conjunction with a 0.5-m focal length Ebert scanning spectrometer (Jarell-Ash Model 82-000) and a linear photodiode array (EG&G 1453) to measure wavelength and spectra. The grating was blazed for 500 nm and had 295 lines/mm. The spectrometer could resolve wavelength peaks to better than 1 nm, but its sensitivity was limited by an f-number of 8.6. Wavelength

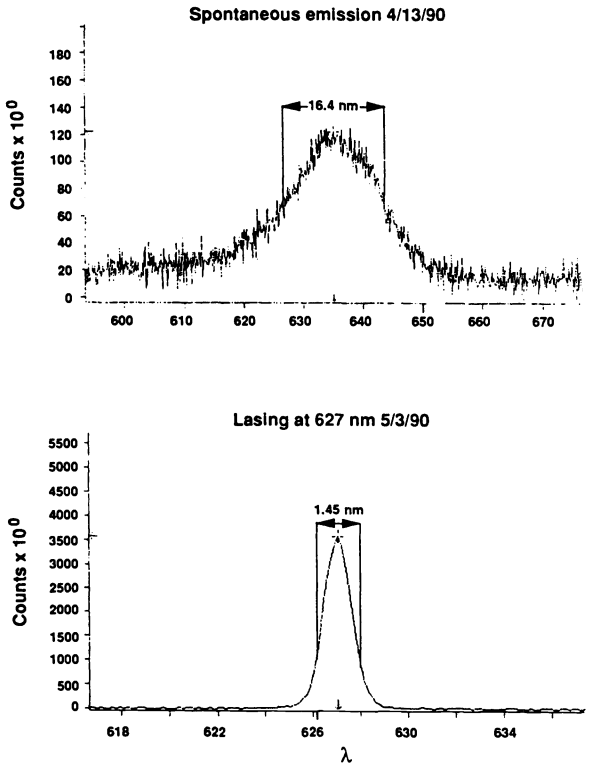

Fig. 10 Wavelength.

measurements were made on the control room diagnostics table shown in Fig. 13 and examples of these measurements are shown in Fig. 10.

The FWHM of the spontaneous emission spectrum for the fundamental harmonic is equal to $\frac{1}{2}N_w$, where N_w is the number of periods in the wiggler. The fractional width of the spontaneous emission spectrum for a wiggler with 220 periods is about 0.25%. The wavelength of the spontaneous emission is related to the electron beam energy, $E_e = \gamma E_{\text{rest}}$, through the following equation:

$$\lambda = (\lambda_w/2\gamma^2)(1 + a_w^2 + \gamma^2\theta^2) \ , \tag{4}$$

where λ_w is the wiggler wavelength and equals 2.18 cm for THUNDER, λ is the FEL wavelength, a_w is the wiggler parameter given by $eB_w\lambda_w/2\pi m_0c^2$ and equals 1.31 for THUNDER, B_w is $B_{\text{rms}}/\sqrt{2}$ for a linear wiggler, θ is the off-axis angle, and E_{rest} is the rest energy of an electron, 0.511 MeV. The FWHM of the spontaneous emission spectrum is a measure of the energy spread of the e-beam according to

$$\Delta\lambda/\lambda = 2\ \Delta E/E \ , \tag{5}$$

where $\Delta\lambda$ is the FWHM of the spontaneous spectrum and $\Delta E/E$ is the fractional energy spread of electron beam. This can be seen from Eq. (4) if the terms a_w^2 and $E_e^2\ \theta^2$ can be ignored, such as in the case when the electron beam is on the wiggler axis. However, if the electron beam is not steered into the wiggler correctly and results in an angular displacement along the optical axis, both a_w and θ increase the width of the spontaneous spectrum. For example, a 0.5 mrad error results in about a 1% increase in λ. Similarly, the field error experienced by the electron beam displaced 0.5 mm (10% of the wiggler bore) from the wiggler axis translates into a 1% increase in λ. When the spontaneous emission spectrum was observed to be larger than that expected in Eq. (4), the electron beam was resteered into the wiggler.

The wavelength of the FEL light was measured to determine the optical extraction and the e-beam energy. The outcoupler that split part of the FEL light out of the ring resonator was wavelength dependent, and therefore, so was the optical extraction. Wavelength measurement errors were less than 1% because of the resolution of the OMA and because a calibrated source was used to check the OMA daily.

8 Pulse Width

The pulse width of the electron beam micropulse was a measure of the performance of the 108 and 433-MHz prebunchers and tapered phase velocity buncher. From the electron micropulse pulse width and the charge in the electron micropulse, the current per micropulse in the wiggler could be calculated. The pulse width of the electron beam micropulses was measured using Cherenkov light created as the electron bunch passed through a quartz screen located between the first two accelerator sections. This light was transported to the control room (see Fig. 13) where its temporal width was measured with a Hamamatsu streak camera (Model C1587 with a fast streak module M1952). Cherenkov light is broadband radiation, and so temporal dispersion of the light pulse through the relay lenses of the optical paths increased the observed pulse width. To avoid this, a low-pass red glass filter was used to limit the bandwidth of light sent to the streak camera. The streak camera provided an on-line tuning aid for the bunchers. Electron pulse width was also measured by using the spontaneous emission from the wiggler.

The optical pulse width of the FEL was used to calculate the FEL output power. Examples of streak camera data are shown in Fig. 11. The pulse width of the electron beam was 10 to 15 ps at the injector, and the FEL pulse length was approximately 9 ps.

The streak camera used for pulse-width measurements was located in the control room. Its temporal resolution was 2 ps and it had an f-number of 1.2. Statistical variations in pulse-width data were about 10% for measurements made over a short period of time. However, some systematic errors may have existed because of beam fluctuations.

9 Time-Resolved Spectroscopy

Time-resolved spectroscopy on the laser light was useful as a diagnostic for the energy slew of the electron beam over a macropulse, and it was the primary diagnostic for indicating the presence of the sideband instability in the FEL resonator.

A monochromator placed in front of a streak camera[2] dispersed the FEL light across the horizontal slit of the streak camera. The streak camera in turn converted the time information in the pulse into a trace along the vertical axis of the video image. A two-dimensional image of time versus wavelength was obtained for the whole macropulse of FEL light. When there was energy slew present in the electron beam, the FEL light could be seen to chirp over the macropulse, as shown in Fig. 12. In Fig. 12 the FEL wave-

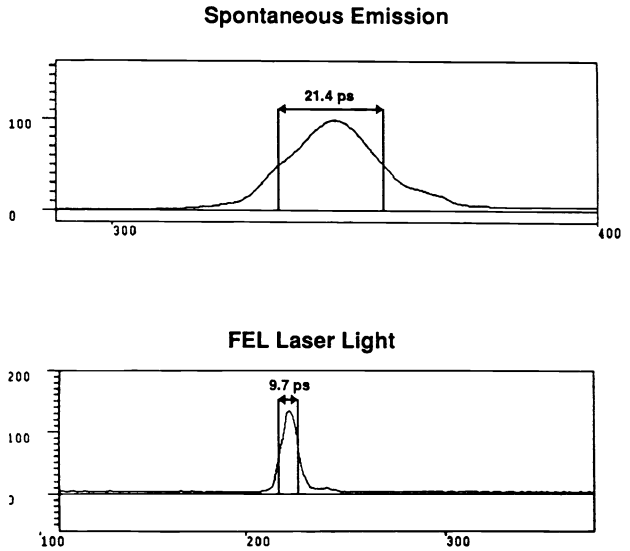

Fig. 11 Pulse length.

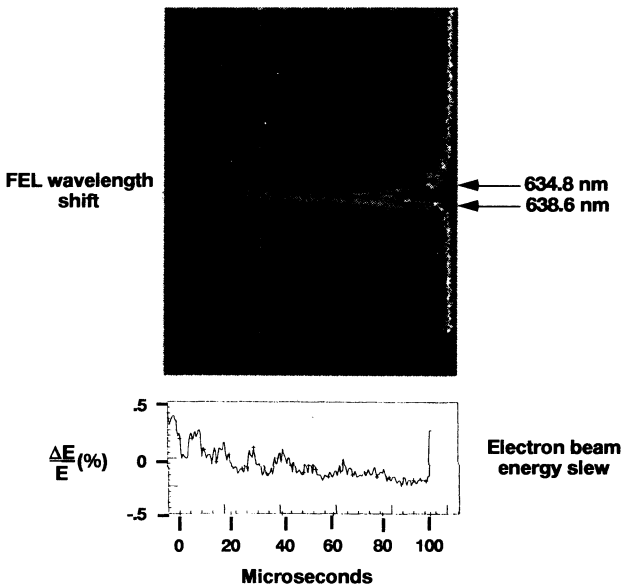

Fig. 12 FEL wavelength shifts with electron beam energy.

length changed from 634.8 nm at the front end of the macropulse to 638.6 nm at the end of the macropulse. This was a 0.6% change in wavelength and can be seen to agree with the measured electron beam energy slew.[7]

10 Detector Layout and Paths

Figure 13 shows the layout for the optical table in the accelerator control room. The reason for not locating the streak camera and OMA in the accelerator chamber was to avoid radiation damage. Also in Fig. 13 is a diagram of the layout for the detectors in the accelerator chamber. A parabolic mirror in combination with another lens formed a reducing telescope for the outcoupled light to the chamber diagnostics table. An attempt was made to minimize the length of the optical path between the outcoupler of the resonator and the detectors in order to minimize optical losses and easily maintain alignment.

There were three diagnostics paths to the control room from the accelerator chamber. One was a path from the outcoupler which made use of a Space Optics Research Labs (SORL) telescope to reduce the 8-in. optical beam from the outcoupler to a beam (1½-in. diam) transportable by 3-in. optics. Another path ran from the retractable mirror downstream of the wiggler and became colinear with the outcoupler path further downstream of the wiggler. A third path began at the Cherenkov station after the first accelerator section and ran independently of the other two paths to the control room. A diagram of the optical paths is shown in Fig. 13.

11 Summary

Table 2 is a summary of each optical measurement discussed, the information that was obtained from it, the detector used, and the errors associated with each measurement. The Rayleigh range and focus position measurements were made at the beginning of an experimental run to check that the optical mode supported by the ring resonator had a waist of the right size near the center of the wiggler. Before injecting the electron beam into the wiggler, the successive passes of the alignment beam around the ring resonator had to be colinear so that the optical mode did not wander off over successive passes when the electron beam was present. At this point, certain electron beam parameters had to be met. The emittance, angular divergence, and spot size of the electron beam at the wiggler were measured to match the beam to the wiggler, after which the electron beam was steered through the wiggler. If the FWHM of the spontaneous emission spectrum was larger than that expected from the energy spread of the electron beam, the electron beam was steered again into the wiggler. If all these parameters were within acceptable limits, the cavity length of the resonator could be varied in small increments in order to search for the onset of lasing. In the case of first lasing, a gross cavity length search was conducted, as described in Sec. 3. When lasing was achieved, energy per micropulse, small signal gain, ringdown, and wavelength were measured to determine the characteristics of the laser. The outcoupled energy per micropulse determined the outcoupled power of the FEL given the wavelength and pulse width of the laser light and transmission of the outcoupler. The measurement of small signal gain (or the FEL gain in the small signal regime) was difficult to make, but is a key FEL parameter. Ringdown loss indicated the combined resonator and electron beam losses in the FEL interaction. Time-resolved spectroscopy was useful as a diagnostic for the energy slew of the electron bunches over a macropulse. The optical measurements and diagnostics evolved over a year of testing the FEL and were essential for the reliable startup, uniform lasing, and characterization of the FEL.

Acknowledgments

The authors thank P. Johnson, K. McCrary, M. Bemes, R. Hawkins, and A. Currie for their dedication and hard work in building, maintaining and operating the FEL, and M. Bailey and D. Schultz for installing and maintaining the optical systems. This work was supported by the U.S. Army Strategic Defense Command under Contract DASG60-87-C-0011.

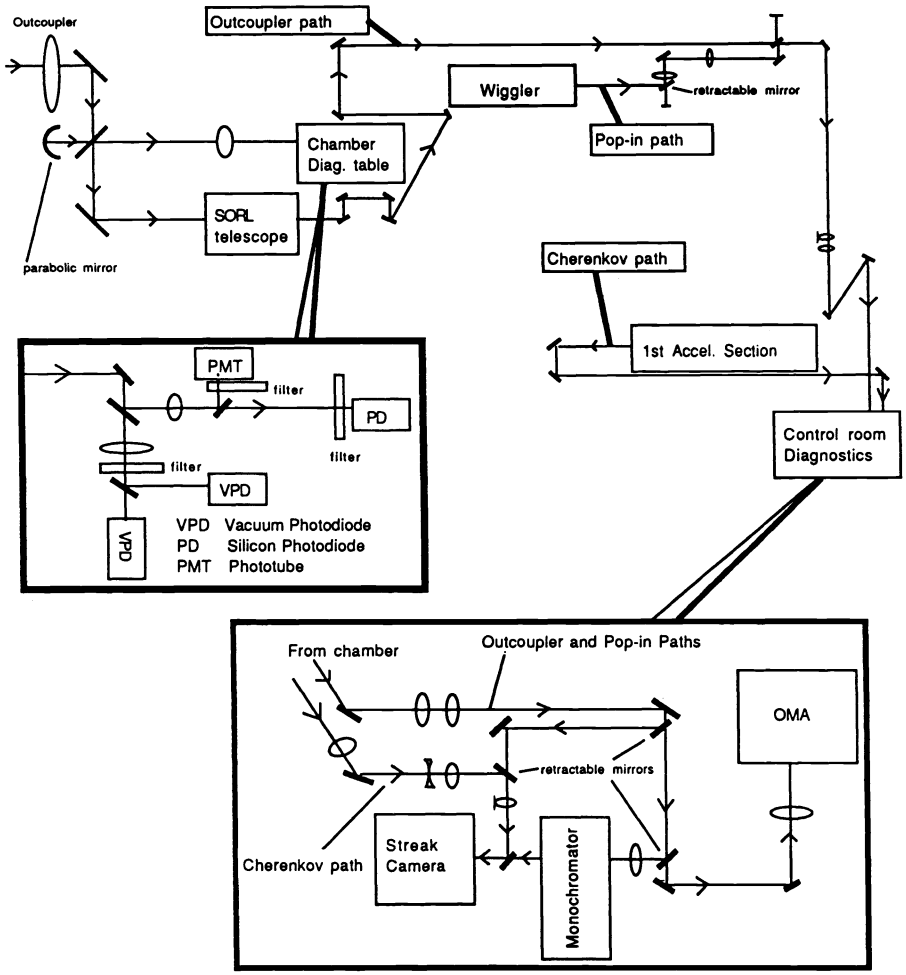

Fig. 13 Optical diagnostics paths.

Dedication

The authors wish to dedicate this paper to the memory of Andrew Richard Lowrey, who led the team that made the first ring resonator FEL LASE. His extraordinary humor, good nature, and expert judgment helped us through the many long days of the FEL experiment. He is greatly missed.

References

1. J. Slater, T. Churchill, D. Quimby, K. Robinson, D. Shemwell, A. Valla, J. Adamski, W. Gallagher, R. Kennedy, B. Robinson, D. Shoffstall, E. Tyson, A. Vetter, and A. D. Yeremian, "Visible wavelength FEL oscillator," *Nucl. Instrum. Methods, Phys. Res. Sect. A* **A250**(1–2) (Sep. 1, 1986); *Free Electron Lasers, Proc. of the Seventh Int. Conf.*, Tahoe City, California, September 8–13, 1985, pp. 228–232.
2. A. H. Lumpkin, R. L. Tokar, D. H. Dowell, A. R. Lowrey, A. D. Yeremian, and R. E. Justice, "Improved performance of the Boeing/LANL FEL experiment: extraction efficiency and cavity length detuning effects," *Nucl. Instrum. Methods,* **A296,**169–180 (1990).
3. R. L. Tokar, L. M. Young, A. H. Lumpkin, B. D. McVey, L. E. Thode, S. C. Bender, K. C. D. Chan, A. D. Yeremian, D. H. Dowell, A. R. Lowrey, and D. C. Quimby, "INEX simulations of the Boeing FEL system," *Nucl. Instrum. Methods* **A296,** 115–126 (1990).
4. J. M. Eggleston and J. Slater, "Baseline conceptual design for high-power FEL ring cavities," *IEEE J. Quantum Electron.* **QE-23**(9), 1527–1533 (1987).
5. S. V. Gunn and K. C. Sun, "Design of ring resonator for burst mode free electron laser," in *AIAA 19th Fluid Dynamics, Plasma Dynamics and Lasers Conference,* 8–10 June 1987.
6. D. H. Dowell, M. L. Laucks, A. R. Lowrey, M. Bemes, A. Currie, P. Johnson, K. McCrary, L. Milliman, C. Lancaster, J. Adamski, D. Pistoresi, D. R. Shoffstall, M. Bentz, R. Burns, J. Guha, R. Hudyma, K. Sun, W. Tomita, W. Mower, S. Bender, J. Goldstein, A. H. Lumpkin, B. McVey, R. Tokar, D. Shemwell, "First operation of a free electron laser using a ring resonator," *Nucl. Instrum. Methods* **A301,** 1–11 (1991).
7. D. H. Dowell, M. L. Laucks, A. R. Lowrey, J. Adamski, D. Pistoresi, D. R. Shoffstall, A. H. Lumpkin, S. Bender, D. Byrd, R. L. Tokar, K. Sun, M. Bentz, R. Burns, J. Guha, and W. Tomita, "Final results of the Boeing and Los Alamos grazing-incidence ring resonator free electron laser experiment," in *Proceedings of the 13th International FEL Conference,* Santa Fe, NM, 25–30 Aug 1991.
8. D. H. Dowell, K. J. Davis, E. L. Tyson, J. L. Adamski, K. D. Fridell, D. R. Shoffstall, A. H. Lumpkin, and H. Takeda, "Electron beam emittance techniques for the average power laser experiment (APLE) injector," in *Proceedings of the 13th International FEL Conference,* Santa Fe, NM, 25–30 Aug 1991.
9. C. G. Parazzoli, R. E. Rodenburg, J. B. Romero, J. L. Adamski, D. J. Pistoresi, D. R. Shoffstall, and D. C. Quimby, "CW 100 kW radio frequency-free-electron laser design at 10 μm," *IEEE J. Quantum Electron.* **27**(12) (1991).
10. J. L. Adamski, W. J. Gallager, R. C. Kennedy, and A. D. Yeremian," A high current injector for the Boeing Radiation Laboratory FEL experiment," *IEEE Trans. Nucl. Sci.* **NS-30**(4) (1983).
11. K. E. Robinson, D. C. Quimby, and J. M. Slater, "The tapered hybrid undulator (THUNDER) of the visible free electron laser experiment," *IEEE J. Quantum Electron.* **QE-23,** 1497–1513 (1987).
12. R. Hudyma and L. Eigler, "Computer-aided alignment of a grazing incidence ring resonator for a visible wavelength free electron laser," in *International Lens Design Conference, Proc. SPIE* **1354,** 523–532 (1990).
13. D. A. G. Deacon, L. R. Elias, J. M. J. Madey, G. J. Ramian, H. A. Schwettman, and T. I. Smith, "First operation of a free-electron laser," *Phys. Rev. Lett.* **38,** 892 (1977).

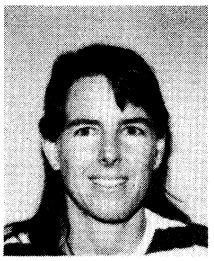

Mary L. Laucks received a BS from the University of California at Santa Barbara in 1980 and an MS from the University of Washington in 1985, both in physics. From 1980 to 1981 she worked on infrared detector development at the Santa Barbara Research Center. She was with the Boeing Free Electron Laser Program from 1987 to 1991 and was responsible for instrumentation of electron beam diagnostics, the design and implementation of optical diagnostics for the ring resonator of the laser, and laser tests. She is presently pursuing a PhD in atmospheric chemistry and global climate change at the University of Washington.

David H. Dowell received the MS and PhD degrees from the University of Illinois, Urbana, in 1974 and 1981, respectively. From 1981 to 1983 he continued postdoctoral studies in nuclear physics at the University of Washington, Seattle. In fall 1983, he became a staff physicist at Brookhaven National Laboratory, Upton, New York. While at Brookhaven, he participated in research at the Tandem Van de Graff Facility, University of Illinois, and University of Mainz, Germany, and planned experiments for the Laser Electron Gamma Source facility then under construction at the National Synchrotron Light Source. Since 1987, he has been with the Boeing FEL Facility, Seattle, Washington.

Andrew R. Lowrey (deceased).

Steven C. Bender: Biography and photograph not available.

Alex H. Lumpkin: Biography and photograph not available.

Melvin P. Bentz received the AA degree in 1971. He has worked in a variety of different fields in research and development, most recently with Rockwell Power Systems, Albuquerque, New Mexico. He worked on the installation, alignment, maintenance, and testing of various high-energy lasers, including the RACHL chemical laser, EMRLD excimers, and the Boeing free-electron laser.